Development of a New Technique to Generate Microcapsules from the Breakup of Non-Newtonian Highly Viscous Fluid Jets

C. Rodríguez-Rivero, E. M. M. Del Valle, and M. A. Galán
Dept. of Chemical Engineering, University of Salamanca, P/Los Caídos S/N, 37008 Salamanca, Spain

DOI 10.1002/aic.12549
Published online March 8, 2011 in Wiley Online Library (wileyonlinelibrary.com).

A new method to produce microcapsules ranging from 300 to 700 μm based on the droplets formation from non-newtonian high viscous liquids has been developed, characterized, and modeled. The technique involves the generation of a continuous high viscous solution jet, which is destabilized by means of a controlled vibration, breaking into droplets that undergo stabilization through a gelling process. Finally, the application of the wave-mechanisms-based theory to obtain a set of equations for the fitting of experimental data is assessed, as a first approximation for a better knowledge of the process. To find the fitting equations, the influence on the microcapsules size is studied through two-dimensionless groups, the Ohnesorge and the Weber numbers, involving the liquid viscosity and flow, respectively, and determining their exponential dependences. Further coefficients are obtained by least-squares fit of the experimental data.
 AIChE J, 57: 3436–3447, 2011
Keywords: jets, Rayleigh-type breakup, viscosity, laminar flow, vibrating nozzle

Introduction

In the last decades, the applications of microencapsulation have increased considerably, especially concerning food,[1] pharmaceutical, bioengineering, and biomedical applications.[2,3] Mainly, some of the reasons are: the microcapsules allow the controlled release of the contained active agent,[4] the masking of flavors, and the mechanical and immune protection of biological principles, such as proteins or living cells.[2,3,5]

The latter application, the microencapsulation of living cells or biomolecules, is the most selective among all of them, as some restrictive requirements concerning toxicity, kinetics formation, mechanical stability, and monodispersion have to be taken into account.[6,7]

Multiple techniques to produce microparticles have been developed, which are usually classified into physico–chemical and mechanical methods.[8] Coacervation and emulsion are common among the first techniques, from which several problems arise regarding size control and hazardous conditions for the active agent. Hence, the use of mechanical processes, combined with gelation methods of stabilization, has become especially relevant and developed, mainly for biomedical applications.[7,9]

However, in some of these mechanical processes difficulties also arise in controlling the size and shape, principally dealing with viscous fluids. For instance, when the spinning disk technique works with high viscosity fluids, it produces satellite drops and high heterodispersion[10]; in the extrusion by coaxial gas flow (airjet), some troubles related to the intrusion of air bubbles and a low throughput present themselves[7] and the jet cutting method works properly but suffers from what is called cut losses.[11]

On the other hand, the techniques concerning the breakup of laminar jets have become really important, and several studies with the aim of getting a better understanding of these processes are being carried out. These methods involve

Correspondence concerning this article should be addressed to E. M. D. Valle at emvalle@usal.es.

Table 1. Viscosity Values in Respect to Alginate Solutions Concentration

% w/w	μ (mPa s)
1	163
1.5	750
2	2300
2.5	3950
3	5540
3.5	14800

the control of the disturbance that a liquid undergoes when emerging from a circular nozzle,[12,13] achieving through this control a good monodispersion of the samples. Experimentally, the jet may be disturbed through several ways: mechanically, piezoelectrically, and acoustically[14–17] or magnetically,[18–20] undergoing Rayleigh-type breakup, widely known amongst others in inkjet printing applications.[21]

Some of the main disadvantages of Rayleigh-type breakup techniques are also problems regarding the work with high viscous fluids and their low productivity rate, though this second inconvenience can be solved with multinozzle systems.[22,23] Current bibliography only reports few studies of systems running with high viscosity fluids, up to 1400 mPa s[24] or 3000 mPa s.[25,26]

To ensure a good mechanical stability of the microcapsules, the viscosity of alginate solutions should reach over 1000 mPa s.[25] With this new system, we have obtained continuous jets up to 14,000 mPa s, though we have only shown in this study experiments up to 2620 mPa s.

Taking into account the restrictions in relation to polymer viscosities, the aim of this study has been, on one hand, the development of a new technique based on Rayleigh-type breakup that allows to work with high viscous liquid jets producing monodisperse microcapsules and, on the other hand, the study of factors affecting the system and the obtaining of a set of semiempirical models which predict the particle size, giving an initial perspective of the instability taking place.

Materials and Methods

Materials

Same batch of sodium alginate, purchased from Sigma Aldrich (alginic acid sodium salt from brown algae medium viscosity, powder) was used during the whole study. All solutions were prepared dissolving sodium alginate in water under hard stirring for 2 h. The required solutions consist of concentrations between 1.0 and 3.5% w/w.

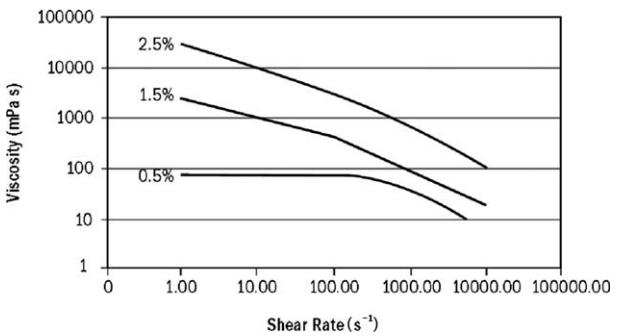

Figure 1. Viscosity values against shear rate.[27]

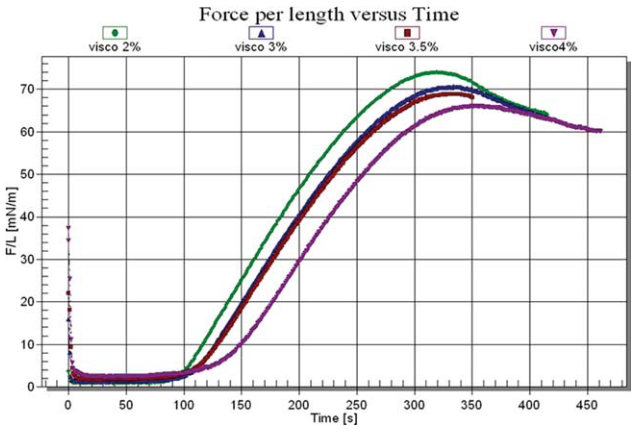

Figure 2. Surface tension values for different concentrations of alginate solutions.

The value decreases slightly when increasing the concentration. [Color figure can be viewed in the online issue, which is available at wileyonlinelibrary.com.]

Barium chloride dihydrate, reagent grade purchased from Scharlau, was used to obtain the hardening solutions dissolving in water in a concentration 2% w/w.

Solutions properties measurements

The viscosity of alginate solutions was determined by using a rotational viscometer (Visco Elite, Fungilab S.A.), at a temperature of 20°C and 6.28 rad/s (60 rpm) with the corresponding spindle in every case (values shown in Table 1). This value for the angular velocity has been chosen constant to following a method of reference for all cases.

The rheology of alginate solutions determines one of the most important physical behaviors of this polymer: its pseudoplasticity, which means that the viscosity of the solution decreases as the shear stresses or shear rate applied increase, as shown in Figure 1.[27]

The surface tension was determined by a tensiometer performing Du Nouy ring measurements (courtesy of Iberlaser S.A. using tensiometer model Sigma 700, KSV), obtaining the values shown in Figure 2. It can be observed that the surface tension values do not almost vary when the polymer concentration changes.

Experimental device

The device that has been optimized to produce microbeads based on a laminar viscous jet breakup induced by a superimposed controlled vibration is shown in Figure 3:

The pneumatic cabinet (2) has been previously designed to develop an air blast atomization technique by Herrero et al.[28] and, for the current application here described, it has the function of supplying and controlling the proper amount of air to pressurize the supply tank (3), fed from the synthetic air cylinder (1). This pneumatic cabinet differentiates this system from commercial devices and allows pushing high viscous solutions towards the nozzle. The nozzle is located in a commercial system that generates the continuous jet (Nisco VARD Encapsulator, Nisco Engineering AG). Both systems are connected through a PVC (polyvinyl chloride) pipe and steel quick connectors.

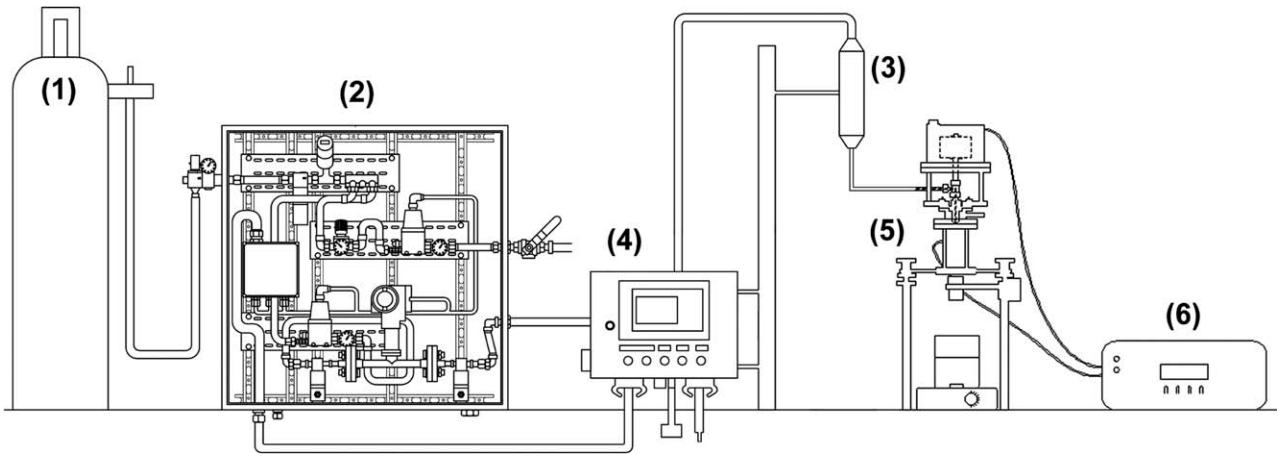

Figure 3. Experimental device to generate monodisperse microcapsules from high viscous non-Newtonian fluids.

(1) Compressed syntethic air cylinder, (2) pneumatic cabinet, (3) pressurized tank, (4) control board, (5) commercial system to impose external perturbation, and (6) frequency and amplitude controller.

Some other authors have also used pressurized air to force the liquid through a nozzle[16,23] but applied to lower viscosity values, whereas others have also carried out similar studies with commercial vibrating nozzles devices.[17,29,30]

The high viscous alginate solution is pushed from the pressurized tank towards the nozzle, producing a steady flow through it. Nozzles with diameters from 50 to 600 μm may be adapted. When a steady flow through the nozzle is achieved the external vibration source, a piezoelectric device connected to the nozzle through a T-piece, produces a controlled disturbance in the thread. The piezoelectric element can generate a vibration from 160 to 10,000 Hz. The applied disturbance destabilizes the jet, disintegrating it in droplets that fall into the barium chloride hardening solution, at a distance of 20 cm from the nozzle. Finally, the microdroplets are maintained in the hardening solution during 10 min to achieve complete membrane solidification.

The formation of droplets can be directly observed through a glass window by means of a stroboscopic light. The parameters of air pressure, which controls the alginate flow rate, and the frequency and amplitude of the superimposed vibration can be controlled by (4) and (5), respectively.

Particle size analysis

The values of particle size and distributions are determined using a particle analyzer (Mastersizer2000, Malvern Instruments) by laser diffraction technology. The size used in the analysis is characterized by the Sauter mean diameter (SMD), which is the diameter of a droplet that has the same volume-surface area ratio as the arithmetic mean of volume-surface area ratio of the total of droplets, this means the diameter of a droplet presenting the same volume-surface area ratio as the ratio of the total volume of droplets and the total surface area. Thus, mathematically expressed:

$$\mathrm{SMD} = \frac{\int_0^\infty D^3 dN}{\int_0^\infty D^2 dN} \tag{1}$$

where D is the droplet diameter, and dN the percentage of the total number of droplets with a diameter contained in the interval $[D, D + dD]$.

After analyzing the size, an image characterization of the particles is carried out using an optical microscope DM1000 Leica (Leica Microsystems) with camera Leica DFC280.

Theory

One of the classical studies in fluid dynamics has been the instability of a capillary liquid jet under the effect of surface tension. When a liquid flows through an orifice or a nozzle at certain velocity, the stream generated at the exit is perturbed simply due to noise, or the way of creating the perturbation can be also specifically imposed. Because of surface tension the disturbance is amplified and, depending on the balance of acting forces, it may grow in time and space. This growth may lead to the break up, which means that the jet breaks into droplets downstream, or it might decay and eventually stabilize.[31]

Plateau[12] observed that a cylindrical jet does not have the minimal surface energy according to the given volume and he noticed that, when the thread splits up in segments $\sim 2\pi$ times its radius, the droplets produced have the minimal surface energy for that volume. Rayleigh[13] came to the same conclusion and used a theoretical linear temporal analysis to determine the optimal wavelength corresponding to the maximal growth rate, though he considered a Newtonian fluid surrounded by an infinite and inviscid fluid. The expression

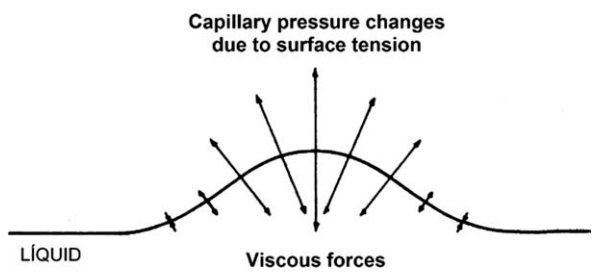

Figure 4. Balance of forces acting in Rayleigh instability.

Table 2. Similarities Between Rayleigh-Type Breakup and Atomization Processes

	Expression in the system	
Theoretical concept: wave mechanism	Atomization	Vibrating nozzle
External perturbation/Disruptive force	Air	Vibration
Type of produced disturbance in the jet or liquid sheet: surface waves	Axisymmetric sinusoidal disturbance in the surface	Axisymmetric sinusoidal disturbance in the surface
Breakup background: increase of the amplitude in the surface waves by turbulences	Aerodynamic pressure	Pressure related to surface tension
Other influential parameters on the amplitude of the surface waves	Viscosity (stabilizing effect)	Viscosity (stabilizing effect)
Dimensionless numbers relevant for the model	Ohnesorge Weber Masic flows ralation	Ohnesorge Weber

that he obtained to calculate the optimal wavelength (when the growth rate of the disturbance is maximum) was:

$$\lambda_{opt} = \pi \cdot \sqrt{2} \cdot d \cong 4.44 \cdot d \tag{2}$$

After Rayleigh, Weber[32] studied viscous fluids and found that, in those cases, the most unstable wavelength was longer than that predicted by Rayleigh studies:

$$\lambda_{opt} = \pi \cdot \sqrt{2} \cdot d \left(1 + \frac{3\mu}{\sqrt{\rho\sigma \cdot d}}\right)^{1/2} \tag{3}$$

Once the optimal wavelength is obtained, the frequency to be applied is calculated as followed:

$$f_{opt} = \frac{v}{\lambda_{opt}} \tag{4}$$

where v is the velocity of the jet.

All mentioned authors concluded that a thread might break up into droplets through a finite wavelength causing an axisymmetric capillary instability. One of the ways to externally create that destabilizing wavelength and control the breakup and monodispersion of samples is by applying a frequency and amplitude controlled disturbance to the flow of liquid forming the jet, in the form of a controlled vibration.

Development of a Semi-Empirical Model to Predict Microparticle Size

Acting forces in Rayleigh instability

The system of forces that acts on the interface of the described system under instability is shown in Figure 4. The viscous forces oppose to the growth of the disturbance as the superimposed vibration produces pressure fluctuations at the interface due to surface tension forces and tends to increase the amplitude of the wave.

Table 3. Viscosity Values in Respect to Alginate Solutions Concentration Used for the Experimentation

% w/w	μ (mPa s)
1.3	450
1.5	750
1.7	1300
1.8	1720
1.9	2000
2	2300
2.1	2620

Wave mechanism theory

As explained before, the disintegration of a liquid laminar jet is a result of internal and external causes. The first ones involve shear stresses, friction, or irregularities in the geometry of the nozzle. The external ones are derived from superimposed disturbances and certain minimal interactions with surrounding air.[33] All of them cause the growth of axisymmetrical sinuous waves at the interface of the stream, having as main acting agents the viscosity and surface tension forces.

In a similar way, atomization processes are also characterized by the flow properties in and out of the atomizers, the surrounding air, and the development of waves at the interface of the jet, controlling the mechanism viscosity and surface tension.[31,34] In the case of atomization processes, the aerodynamical forces and the geometry of the nozzle are more relevant than those in processes based on Rayleigh-type breakup, being that the aerodynamical forces in these processes usually neglected. In Table 2, the basic characteristics and parameters affecting both instabilities, laminar jet breakup and atomization processes, are compared, where several similarities can be seen.

Therefore, considering the wide acceptance that the wave mechanism theory has among the atomization processes, its application to the new technique described has been studied as a first approximation.

This theory describes the disintegration process caused by the growth of unstable waves at the liquid–gas interface, when the air interacts with the liquid, being these waves generated by pressure fluctuations or turbulences in the gas or liquid streams.[35] The waves continue as capillary waves if the surface tension predominates or as acceleration wave when the pressure forces predominate.[36]

Thus, Adelberg,[35,37] Jeffreys,[38] and Mayer[39] studied wind-induced instabilities and found that the amplitude of the

Table 4. Experimental Conditions in Which Set-Up Experiments have been Carried Out

Alginate viscosity (mPa s)	450–2620
Alginate flow rate (cm^3/min)	5–9
Surface tension (N/m)	0.076
Nozzle diameter = jet diameter (μm)	150
Density (kg/m^3)	1000
Reynolds number	0.29–2.32

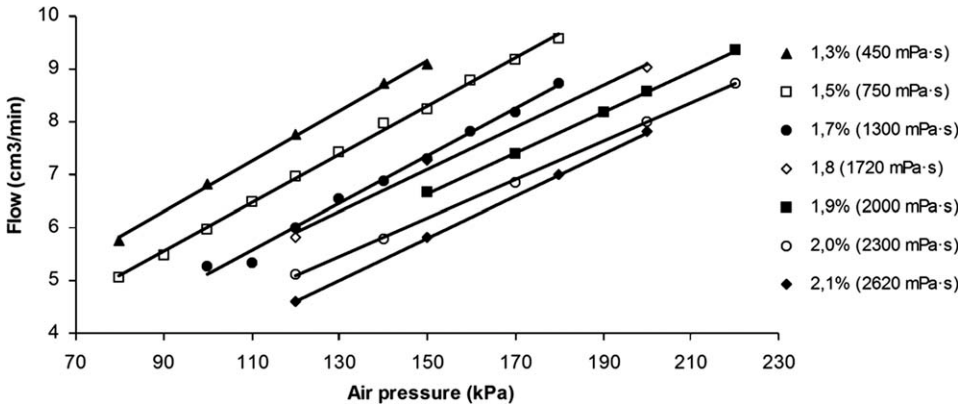

Figure 5. Relation between pressure imposed inside the tank by means of compressed air and the flow of alginate solutions of different concentrations.

waves at the interface grows when exceeding a minimum value and, when becoming large enough, the jet breaks. The expression describing the amplitude of surface waves is:

$$\frac{dA}{dt} = A\left[\frac{\pi\beta\rho_a(U_a - u)^2}{\lambda\rho_l u} - \frac{8\pi^2\mu_l}{\rho_l\lambda^2}\right] \tag{5}$$

From the expression (5), it can be seen that the amplitude is damped by the viscosity—tending to stabilize the instability—as it increases as the difference between the gas and liquid phases velocities increases.

When the aerodynamic pressure force and the surface tension forces are significant, the velocity of the wave u is given by:

$$u = \left[\frac{a\lambda}{2\pi} + \frac{2\pi\sigma}{\lambda\rho_l}\right]^{1/2} \tag{6}$$

Being the acceleration due to the aerodynamic drag:

$$a = \frac{4C_{Do}\sin^2\zeta}{\pi D\rho_l}\left(\overline{\rho_a}\overline{U_a^2}/2\right) \tag{7}$$

Substituting (6) and (7) in (5):

$$\frac{dA}{dt} = A\left[\frac{\pi\beta\rho_a U_a^2}{\lambda\rho_l\left[\frac{a\lambda}{2\pi} + \frac{2\pi\sigma}{\lambda\rho_l}\right]^{1/2}} - \frac{8\pi^2\mu_l}{\rho_l\lambda^2}\right] \tag{8}$$

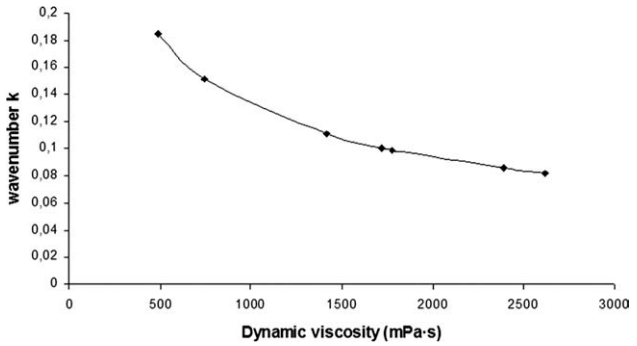

Figure 6. Values of the wavenumber for the different analyzed solutions.

From which can be concluded that surface tension and viscosity oppose to the growth of the instability. The minimum wavelength above which the amplitude grows exponentially with time can be determined by $dA/dt = 0$, leading to the expression:

$$\lambda_m^2 - \lambda_a\lambda_m^2 - \lambda_\sigma^2 = 0 \tag{9}$$

$$\text{With}: \quad \frac{\lambda_\sigma}{D} = \frac{2\pi(16)^{1/3}}{\beta^{2/3}}(Z/We)^{2/3} \tag{10}$$

where λ_σ the wavelength of capillary waves

$$\frac{\lambda_a}{D} = \frac{64C_{Do}\sin^2\zeta}{n*\beta^2\pi}(Z^2/We) \tag{11}$$

where λ_a the wavelength of acceleration waves and

$$n* = \rho_a U_a^2/\overline{\rho_a}\overline{U_a^2}$$

the shock dynamic pressure ratio

When aerodynamic pressure forces predominate waves propagate as acceleration waves at a minimum wavelength $(a\lambda_m/2\pi)^{1/2}$. In this case, $\lambda_a \ll \lambda_\sigma$ and the solution of the Eq. 9 is $\lambda_m = \lambda_\sigma$, which is governed by $(Z/We)^{2/3}$.

On the other hand, when the surface tension dominates the waves propagate as capillary waves at a minimum velocity of $(2\pi\sigma/\lambda_m\sigma_l)^{1/2}$. Being thus $\lambda_\sigma << \lambda_a$, a solution for the Eq. 9 is $\lambda_m = \lambda_a$, governed by (Z^2/We).

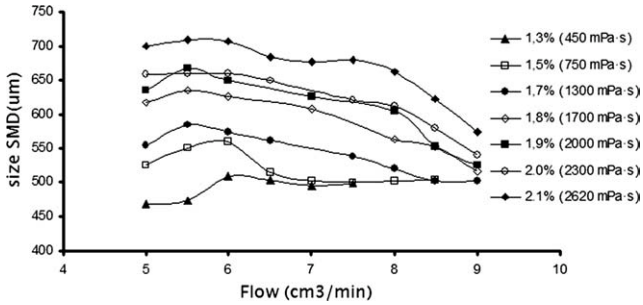

Figure 7. System behavior curves for nine different flows and seven viscosities.

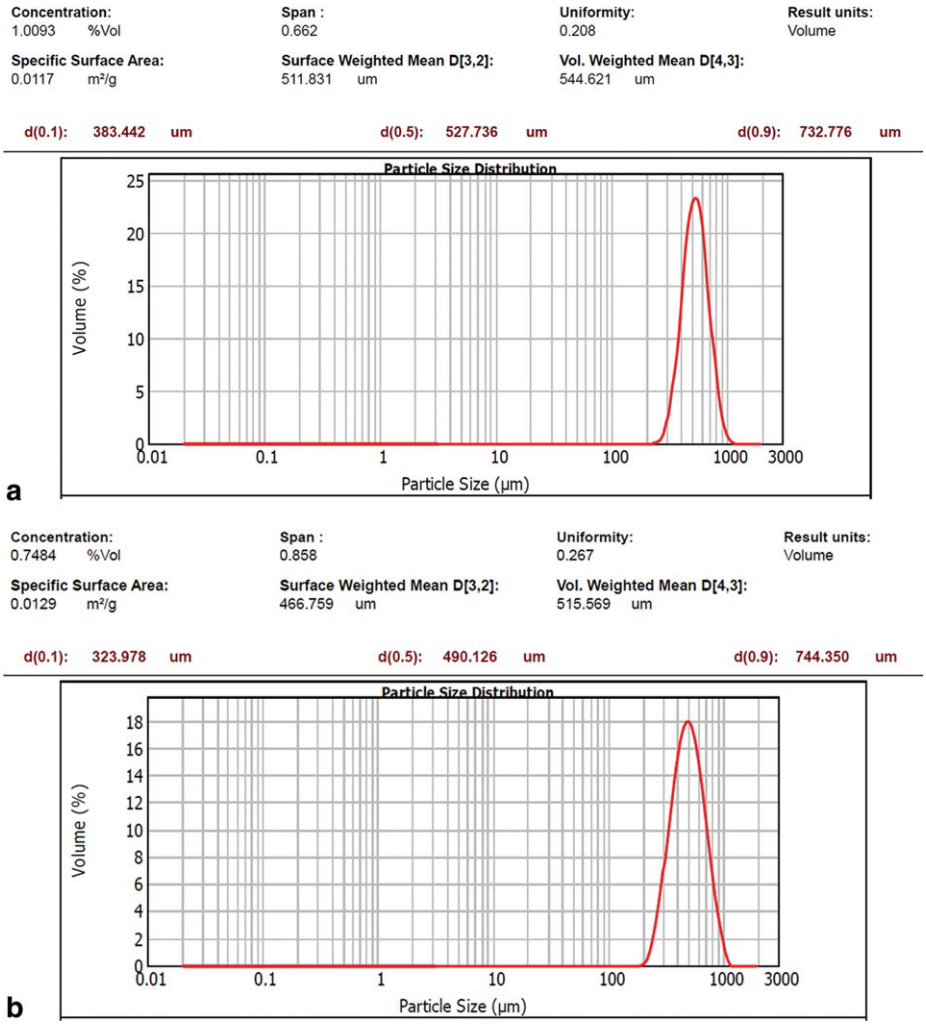

Figure 8. Size distributions (a) for capsules from 1.9% alginate and (b) for capsules from 1.7% alginate, both issuing from a 150 μm nozzle.

[Color figure can be viewed in the online issue, which is available at wileyonlinelibrary.com.]

Summarizing, both dimensionless numbers, *We* and *Z*, have either the same exponents or *Z* exponent is twice that of *We*'s. This is the reason why both will be considered and analyzed through the development of the semi-empirical model.

Set-Up Studies

The new system allowed us to create a continuous jet up to 14,000 mPa s approximately, though for such viscosity values some obstacles affected the system, first difficulties to observe visually the breakup appeared and secondly, the plugging of the nozzle sometimes was becoming a problem after generating such high viscous jets (around 14,000 mPa s) during a long period of time, probably due to solidification of the polymer in the nozzle. The first problem will be solved by acquiring a high speed camera to analyze properly the breakup when increasing the viscosity of the solutions and concerning the plugging we have checked that this effect is well minimized applying ultrasounds and maintaining a proper cleanliness of the nozzle.

Therefore, the viscosity used in the set-up experiments was lowered up to 2620 mPa s, as waiting for the acquisition of a high speed camera which permits the capture of the breakup. In Tables 3 and 4, the experimental conditions are summarized.

The flow tested range from 5 to 9 cm^3/min, which corresponds to the impossibility of creating a steady jet below 5 cm^3/min and the appearance of deformations in the capsules when increasing the flow over 9 cm^3/min, overall for viscosities below 2000 mPa s, due to the high energy in the impact, which will also be named later. On the other hand, the tested viscosities are above 260 mPa s, maximum value that could be processed previously with the commercial device, and below 2700 mPa s due to difficulties described before.

The frequency to be applied can be calculated knowing the physicochemical parameters of the alginate solution, the nozzle diameter, and the jet velocity. In our studies, we have considered the use of Weber equation to determine the optimal wavelength, and then obtaining the frequency to be applied with the velocity of the thread by means of the expressions (3) and (4).

Nozzle flow properties

Depending on the physical properties of the solutions and the air pressure applied to generate the stream, the frequency for the breakup changes, corresponding to the Weber expression shown before (3) and (4).

The flow regime is always laminar and in a jetting mode, not dripping, as Reynolds numbers clearly indicate with very low values, from 0.29 to 2.32, due to the high viscosities.

The liquid flow through the nozzle, this is the jet velocity, is controlled by regulating the pressure inside the pressurized reservoir. The first parameter is determined experimentally, by measuring the amount of alginate collected in a certain period of time and calculating the volumetric flow rate as $F = m/\rho$ (where m is the mass flow rate and ρ the density of the fluid). The velocity of the jet is obtained by the expression $v = F/\pi r^2$ (where r is the jet radius, in our study, it is considered the same as the nozzle radius).

It can be seen in Figure 5, as expected, that an increase in the incoming air pressure is needed in order to provoke an increase in the flow. It is also logic that an increase in the viscosity involves higher air pressures.

Breakup properties

The frequency applied, as mentioned before, corresponds to Weber expressions (3) and (4). It was checked that, for the corresponding values, the breakup always happened, though the wavenumber ranges between 0.082 and 0.18 for the different solutions studied, this is, as Figure 6 shows, increasing the viscosity the wavelength also increases, decreasing the frequency to be applied.

$$k = \frac{2\pi}{\lambda}$$

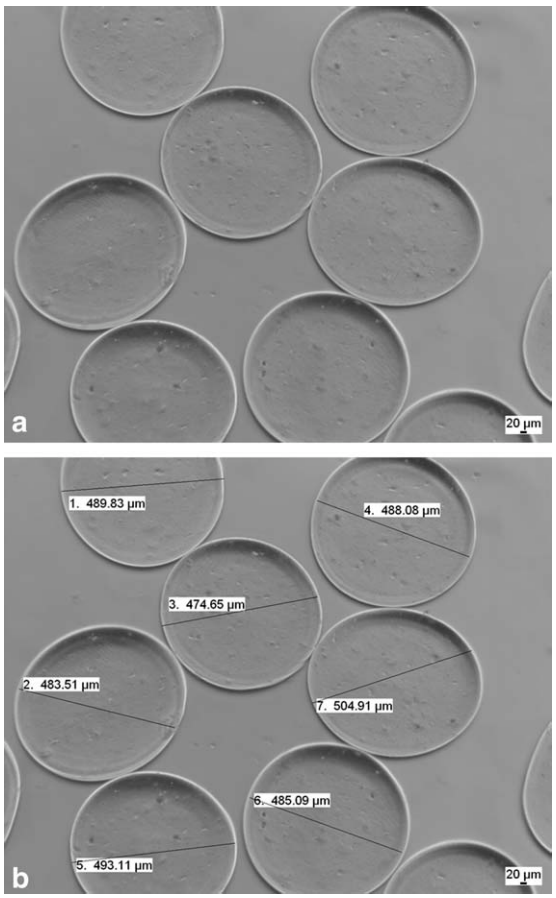

Figure 9. Microphotographs of capsules from alginate 1.8% in concentration (a) as captured from the camera (b) measured by means of the software.

Results and Discussion

Behavior curves

To study the behavior of the system several experiments were carried out, analyzing different flow and viscosity conditions, considering the limitations described previously. Thus, seven viscosities (420–2620 mPa s) and nine different flow regimes (5–9 cm^3/min) were tested, collecting the data in Figure 7, where size is plotted against flow and different behaviors can be distinguished.

From Figure 7, it can be seen as a general behavior that the particle size increases when increasing the viscosity. Observing flows below 6 cm^3/min, the tendency seems to indicate that the particle size increases with the flow, but on the other hand, above 6 cm^3/min we can observe two different behaviors: the first one for solutions with viscosities below 800 mPa s, where the size remains constant as increasing the flow, and second, for solutions with viscosities above 800 mPa s, where the size clearly decreases with the increase of the flow. This latter behavior is the one that we have studied more deeply.

From these results, it can be concluded that the viscosity acts as a stabilizing force, this is it damps the instability out, as it has been reported in several studies. Furthermore, the figure shows a special behavior that clearly differs from other similar studies, this is the decreasing of size when increasing the flow, which proposes the special relevance that pseudoplastic behavior takes in the system. The reason why that performance takes place seems to be the increase of shear stresses in the nozzle when rising the flow, what makes the viscosity of the fluid to decrease, and consequently also the size.

Particle size distribution and image characterization

From the measurements taken by laser diffractometry, the particle size distributions are obtained. The software used gives the span factor of the measured sample, defined as:

$$\text{span factor} = \frac{D_{0.9} - D_{0.1}}{D_{0.5}}$$

where $D_{0.9}$ is the diameter of the 90th percentile, $D_{0.1}$ the diameter of the 10th percentile, and $D_{0.5}$ the diameter of the 50th percentile.

In general, the relative span factor falls within 0.600 and 0.900 as shown in Figure 8.

Several microimages were taken, using the optical microscope DM1000 Leica with an integrated Leica DFC280 camera, to evaluate visually the size and shape of the microparticles. The images were kept by means of

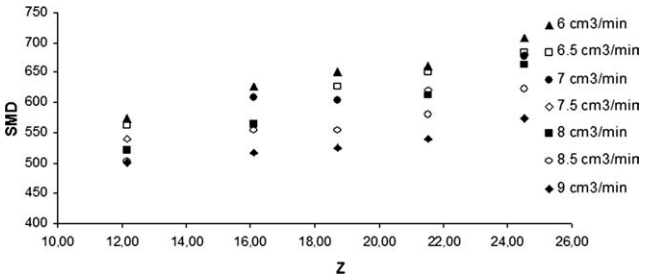

Figure 10. Variation of SMD with Ohnesorge number.

specific Leica IM50 software. An example is shown in Figure 9.

Influence of viscosity on SMD

The liquid properties of the polymer are described by using the Ohnesorge number (Z), which relates the importance of viscous forces to surface tension forces. The Ohnesorge number is expressed by the following equation:

$$Z = \frac{\mu}{\sqrt{\rho \cdot \sigma \cdot D}} \tag{12}$$

Figure 10 collects the experimental SMD values obtained under different Ohnesorge numbers. It can easily be seen that the size increases with the viscosity as shown before. An exponential dependence can be obtained from Figure 11, being the type: SMD $= f(Z^{X_Z})$, obtaining finally SMD $= f(Z^{0.2817})$.

Obtaining a positive dependence of the Ohnersorge number on SMD determines that increasing the affecting properties, in this case, the viscosity (the rest of parameters are considered constant) makes larger the capsules diameter.

Influence of flow on SMD

In a similar way, the flow regime is characterized by the Weber number, which relates inertial forces of the jet with liquid surface tension.

$$We = \frac{\rho \cdot u^2 \cdot D}{\sigma} \tag{13}$$

From Figure 12, it can be seen that the size decreases when increasing the Weber number due to an increase in the flow, as expected and explained in Figure 7.

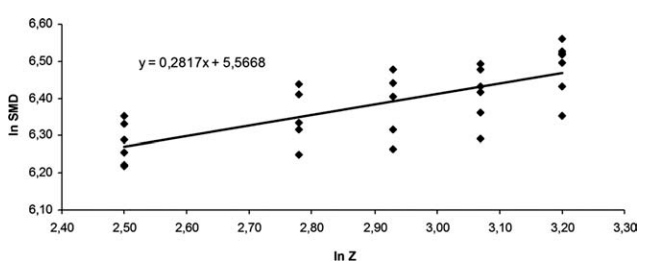

Figure 11. Influence of the Ohnesorge number on the SMD of the microcapsules.

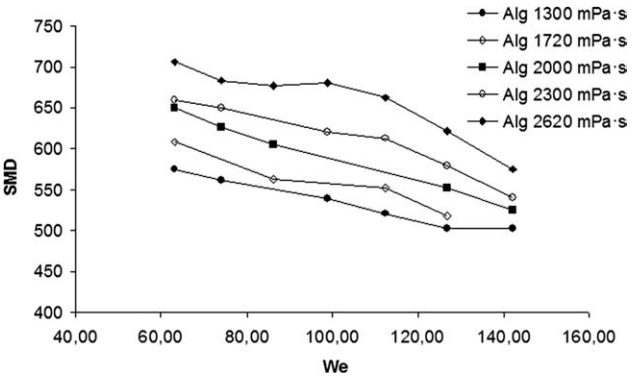

Figure 12. Variation of SMD with Weber number.

Collecting the data, the exponential dependence between Weber number and size can be obtained by the linear expression calculated from Figure 13, obtaining a value: SMD $= f(We^{-0.2247})$.

Obtaining a negative dependence of the Weber number on SMD implies that the higher is the velocity or flow rate of the fluid, the smaller is the capsules size.

Semi-empirical models

As it has been described above, the alginate is a pseudoplastic fluid and this nature seems to become apparent through the behavior that is being studied. However, it has been considered a constant viscosity for each solution, not being the zero shear viscosity or the apparent viscosity for the different flow velocities (with their associated different shear conditions), but a representative value. The reason why the pseudoplastic nature of the polymer has not been taken into consideration for the development of the semi-empirical model is that we first want to check, as a first approach, whether the equations proposed from the wave mechanism, not considering the non-Newtonian terms but a constant viscosity value, agree with our system. Thus, this approach has been considered for us as a first basic knowledge of the behavior of the system.

After the development of this semi-empirical model, we will develop a theoretical analysis in which non-Newtonian terms will be considered and its agreement will be checked also using rheological measurements by means of a rheometer.

Based on wave mechanism theory and selecting from models that Mansour and Chigier[36] propose, the equations collected in Table 5 are studied to determine the agreement with experimental data obtained from this study.

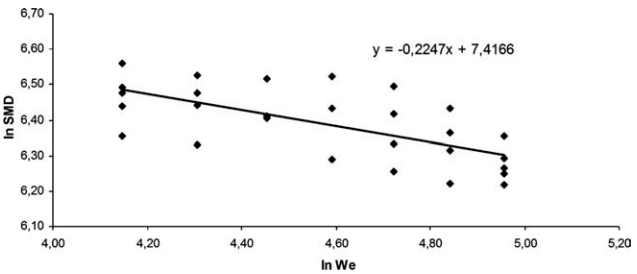

Figure 13. Influence of the Weber number on the SMD of the microcapsules.

Table 5. Proposed Equations to Fit the Data

$$\frac{\text{SMD}}{D} = X_2 We^{-X_1} + X_3 Z^{X_1} + C \quad (14)$$

$$\frac{\text{SMD}}{D} = X_2 We^{-X_1} + X_3 Z^{2X_1} + C \quad (15)$$

$$\frac{\text{SMD}}{D} = X_2 \left(\frac{Z}{We}\right)^{X_1} \quad (16)$$

For Eqs. 17 and 19 both dimensionless numbers have same exponent values, as described before this implies that waves propagate as acceleration waves, predominating aerodynamic pressure forces.

In the case of (18), exponent X_Z is double than exponent X_{We}, which means that surface tension forces predominate, hence the waves propagate as capillary waves.

After substituting the exponential dependence values: $\text{SMD} = f(Z)^{0.2817}$ and $\text{SMD} = f(We)^{-0.2247}$ as well as considering the correlation exponent X_1 by calculating its mean value: $X_1 = (0.2817 + 0.2247)/2 = 0.2532$, according to the experimental data, the unknown coefficients X_2, X_3 in proposed Eqs. 17–19 are calculated through multiple linear regression analysis obtaining the values shown in Table 6 and the equations below

Table 6. Unknown Coefficients for the Eqs. 17–19

	X_2	X_3	C
Equation 17	10.6210	2.0898	−3.7324
Equation 18	10.6203	0.5077	−1.5909
Equation 19	6.0474	–	–

$$\frac{\text{SMD}}{D} = 10.6210 \cdot We^{-0.2532} + 2.0898 \cdot Z^{0.2532} - 3.7324 \quad (17)$$

$$\frac{\text{SMD}}{D} = 10.6203 \cdot We^{-0.2532} + 0,5077 \cdot Z^{0.5064} - 1.5909 \quad (18)$$

$$\frac{\text{SMD}}{D} = 6.0474 \cdot \left(\frac{Z}{We}\right)^{0,2532} \quad (19)$$

Comparison between the experimental size of microparticles and the predicted size by the model

A set of experiments is carried out to compare the experimental data with those predicted by the equations obtained from the

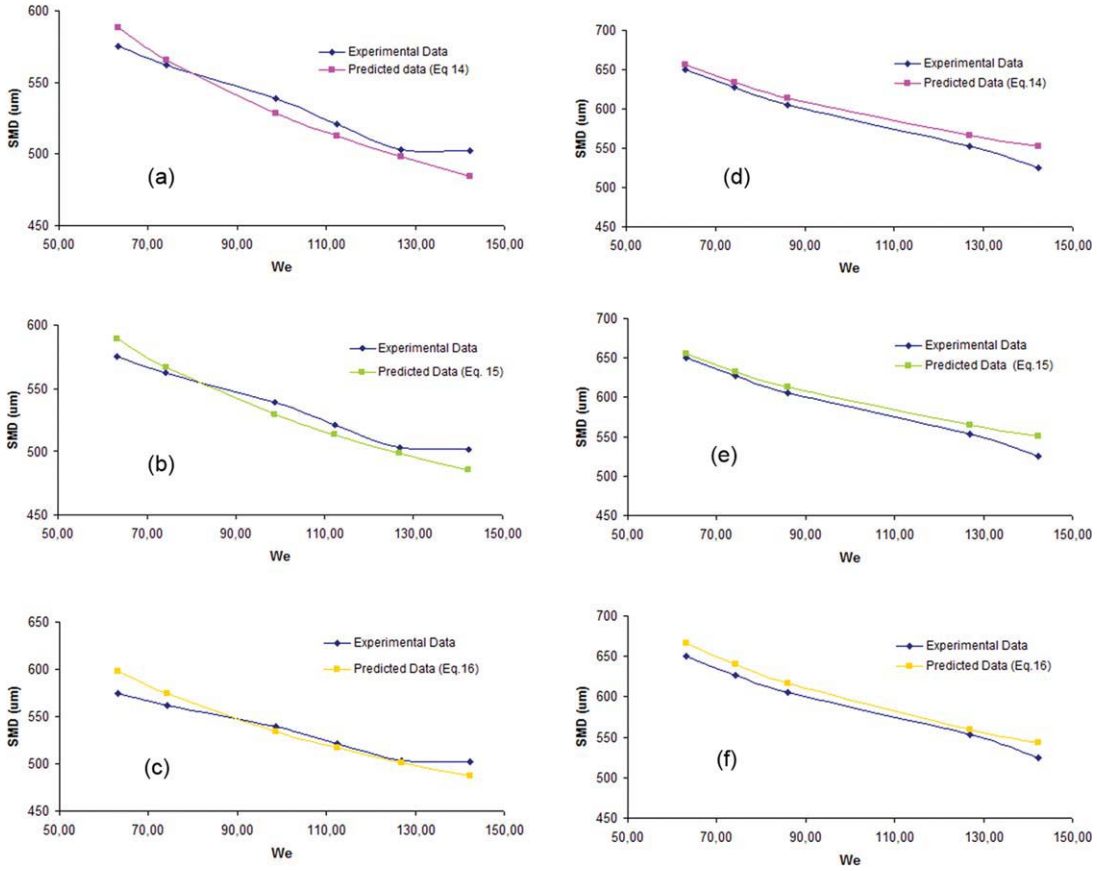

Figure 14. Comparison between experimental and predicted sizes.

[Color figure can be viewed in the online issue, which is available at wileyonlinelibrary.com.]

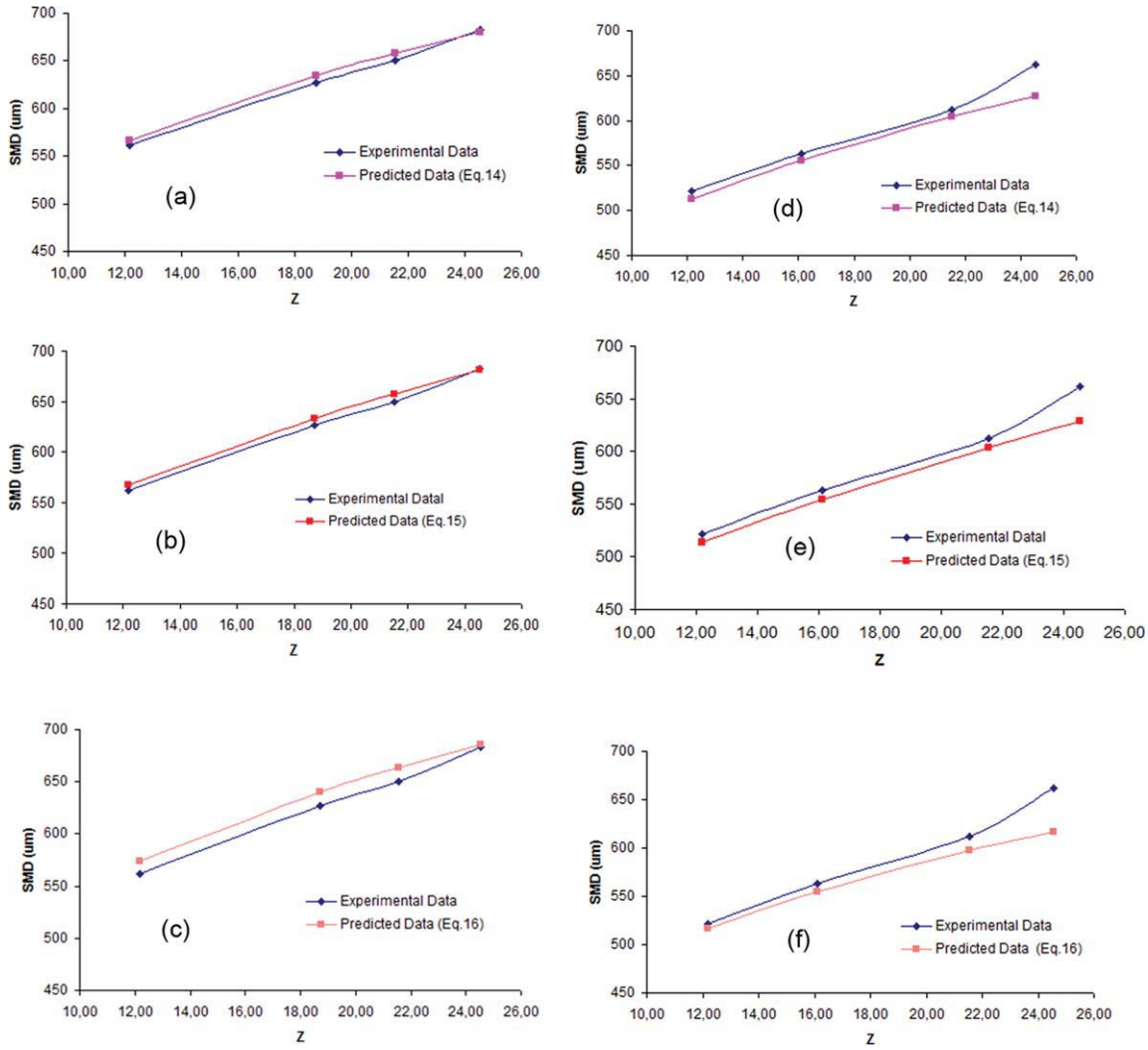

Figure 15. Comparison between experimental and predicted sizes.

At a constant flow of 6.5 cm^3/min (a–c). At a constant flow of 8 cm^3/min (d–f). [Color figure can be viewed in the online issue, which is available at wileyonlinelibrary.com.]

wave mechanism theory. First set of data is taken at constant value for the viscosity for different flows, this is variable Weber, in Figure 14.

A second set of comparative data is taken at constant flow—Weber—and different viscosities, this is variable Ohnesorge, as shown in Figure 15.

In general, it can be concluded that all three proposed equations predict microparticle size with a good agreement with the experimental data, though finding some deviations under certain conditions described next.

After analyzing the value of errors for the different data, it can be observed that the dispersion in the data is wider for the highest flows and the fitting of predicted data is consequently worse than considering medium flow values. That is due to the high energy when capsules impact in the hardening solution, provoking their deformation and reducing the reliability of measurements, increasing errors, as shown in Figures 16a–c.

Second, errors can also be observed for the highest of the viscosity analyzed, 2620 mPa s, what can be produced due to the difficulty to observe visually the breakup of the jet, probably incurring in the use of non optimal breakup frequencies, which leads to heterodispersion, producing higher errors as shown in Figures 16d–f.

Hence, it can be finally concluded that all three equations acceptably predict, under our study conditions, the size of particles. Errors between experimental and predicted size are collected in Table 7. Thus, it seems to be demonstrated that wave mechanism, accepted for non-Newtonian liquids atomization, can also be applied to the new system developed, which allows relating some basic physical parameters through these semi-empirical equations, acquiring a better knowledge of the process.

Conclusions

This study reports the development of a new technology able to generate polymeric microparticles, ranging from 300 to 700 μm in size with high monodispersión, from high viscous polymers. From the experiments here reported, it can be concluded that the new technology developed succeeded in working with high

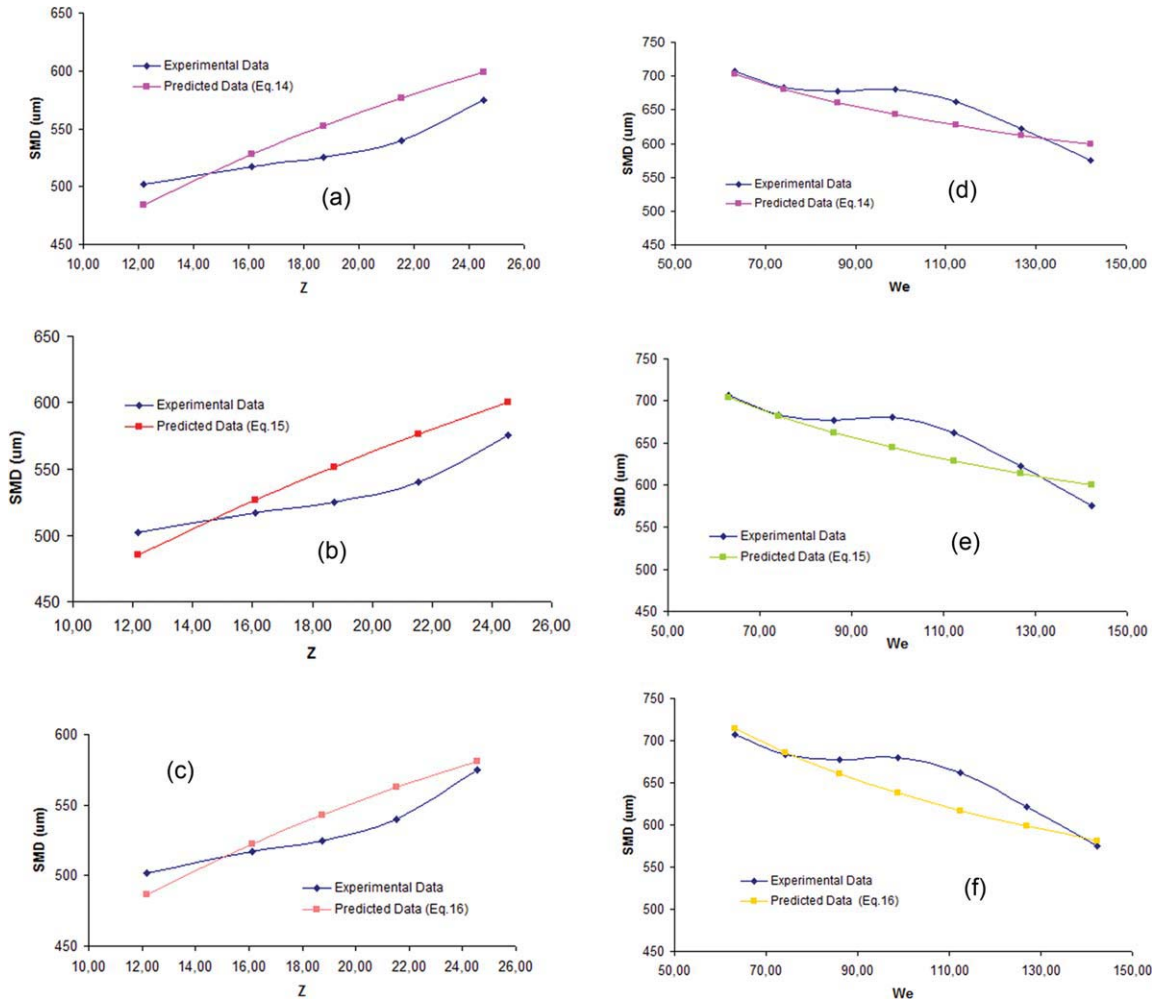

Figure 16. Comparison between experimental and predicted sizes.

Deviations (a–c) at a constant flow of 9 cm^3/min. At a constant viscosity of 2620 mPa s (d–f). [Color figure can be viewed in the online issue, which is available at wileyonlinelibrary.com.]

viscous solutions, creating continuous jets up to 14,000 mPa s. We also verified the stabilizing behavior of the viscosity, as expected, and the special relevance of the pseudoplasticity of alginate.

Besides the development and characterization of the system, a semi-empirical model stemming from the wave mechanism theory has been developed to predict microparticle size. It has been concluded that the obtained equations predict the size of particles acceptably, demonstrating that wave mechanism, accepted for non-Newtonian liquids atomization, can also be applied to the new system developed.

Table 7. Error Values Between Experimental and Predicted Size Using the Semiempirical Equations

	Equation 17	Equation 18	Equation 19
Lowest error (%)	0.14	0.17	0.17
Highest error (%)	6.71	6.65	6.78
Average error (%)	2.25	2.17	2.36

Acknowledgments

This research was supported by funds from the Ministerio de Ciencia e Innovación (Spain), project CTQ2009-08222 (PPQ subprogram). Cristina Rodríguez is also supported by a F.P.U. grant from the Ministerio de Ciencia y Innovación (Spain). This grant is also appreciated by the author.

Notation

A = amplitude of the surface disturbance
C_{Do} = Drag coefficient of a cylinder in cross flow
D or d = jet diameter, considered the same as jet nozzle
F = volumetric flow rate
f = frequency of the disturbance
k = wavenumber
m = liquid mass flow rate
U = air average velocity
u = velocity of the wave
v = velocity of the liquid
We = Weber number
Z = Ohnesorge number
X_{We} = power dependence of SMD on Weber number
X_Z = power dependence of SMD on Ohnesorge number
X_1 = general correlation exponent
$X_{2,3}$ = general correlation coefficients

Greek letters

β = Jeffrey's sheltering parameter
λ = wavelength
ρ = density of the jet
σ = surface tension
ζ = angle between the jet axis and gas
μ = dynamic viscosity

Literature Cited

1. Gouin S. Microencapsulation: industrial appraisal of existing technologies and trends. *Trends Food Sci Technol*. 2004;15:330–347.
2. Hernández RM, Orive G, Murua A, Pedraz JL. Microcapsules and microcarriers for in situ cell delivery. *Adv Drug Delivery Rev*. 2010;62:711–730.
3. Chang TMS, Prakash S. Therapeutic uses of microencapsulated genetically engineered cells. *Mol Med Today*. 1998;4(5):221–227.
4. Venkatesan P, Manavalan R, Valliappan K. Microencapsulation: a vital technique in novel drug delivery system. *J Pharm Sci Res*. 2009;1:26–35.
5. Teramura Y, Iwata H. Bioartificial pancreas. Microencapsulation and conformal coating of islet of Langerhans. *Adv Drug Delivery Rev*. 2010;62:827–840.
6. Peirone M, Ross CJD, Hortelano G, Brash JL, Chang PL. Encapsulation of various recombinant mammalian cell types in different alginate microcapsules. *J Biomed Mater Res*. 1998;42:587–596.
7. Koch S, Schwinger C, Kressler J, Heinzen C, Rainov NG. Alginate encapsulation of genetically engineered mammalian cells: comparison of production devices, methods and microcapsule characteristics. *J Microencapsul*. 2003;20:303–316.
8. Poncelet D. *Microencapsulation: fundamentals, methods and applications*. In: Blitz J, Gun'ko V, editors. *Surface Chemistry in Biomedical and Environmental Science*. The Netherlands: Springer, 2006:23–34.
9. DeGroot AR, Neufeld RJ. Encapsulation of urease in alginate beads and protection from α-chymotrypsin with chitosan membranes. *Enzyme Microb Technol*. 2001;29:321–327.
10. Senuma Y, Lowe C, Zweifel Y, Hilborn JG, Marison I. Alginate hydrogel microspheres and microcapsules prepared by spinning disk atomization. *Biotechnol Bioeng*. 2000;67:616–622.
11. Prüsse U, Bruske F, Breford J, Vorlop KD. Improvements to the jet cutting process for manufacturing spherical-particles from viscous polymer solutions. *Chem Ing Technol*. 1998;70:556–560.
12. Plateau J, editor. *Statique expérimentale et théorique des liquides soumis aux seules forces moléculaires*. Paris: Gauthier-Villars, 1873.
13. Rayleigh L. On the capillary phenomena of jets. *Proc R Soc London*. 1879;29:71–97
14. Bousfield DW, Stockel IH, Nanivadekar CK. The breakup of viscous jets with large velocity modulations. *J Fluid Mech*. 1990;218:601–617.
15. Chaudhary KC, Redekopp LG. The nonlinear capillary instability of a liquid jet, part 1. Theory. *J Fluid Mech*. 1980;96:257–274.
16. Rutland DF, Jameson GJ. Theoretical prediction of the sizes of drops formed in the breakup of capillary jets. *Chem Eng Sci*. 1970; 25:1689–1698.
17. Berkland C, Kim K, Pack DW. Fabrication of PLG microspheres with precisely controlled and monodisperse size distributions. *J Controlled Release*. 2001;73:59–74.
18. Chandrasekhar S, editor. *Hydrodynamic and Hydromagnetic Stability*. Oxford: The Clarendon Press, 1961.
19. Zeleny J. On the conditions of instability of electrified drops, with applications to the electrical discharge from liquid points. *Proc Cambridge Philos Soc*. 1915;18:71–83
20. Zeleny J. Instability of electrified liquid surfaces. *Phys Rev*. 1917; 10(1):1–6.
21. Heinzl J, Hertz CH. *Ink-jet printing*. In: Hawkes PW, editor. *Electronics and Electron Physics*, Vol. 65. Orlando, Florida: Academic Press, Inc., 1985:91–166.
22. Brandenberger H, Widmer F. A new multinozzle encapsulation/immobilisation system to produce uniform beads of alginate. *J Biotechnol*. 1998;63:73–80.
23. Brenn G, Helpio T, Durst F. A new apparatus for the production of monodisperse sprays at high flow rates. *Chem Eng Sci*. 1997; 52:237–244.
24. Wissema JG, Davies GA. The formation of uniformly sized drops by vibration-atomization. *Can J Chem Eng*. 1969;47:530–535.
25. Moghadam H, Samimi M, Samimi A, Khorram M. Electro-spray of high viscous liquids for producing mono-sized spherical alginate beads. *Particuology*. 2008;6:271–275.
26. Watanabe H, Matsuyama T, Yamamoto H. Experimental study on electrostatic atomization of highly viscous liquids. *J Electrostat*. 2003;57:183–197.
27. ISP Pharmaceuticals, Inc. Alginate for Pharmaceutical and Medical Applications. *Performance Enhancing Products. ISP Pharmaceuticals Product Guide*. USA. 2008.
28. Herrero EP, Valle EMMD, Galán MA. Development of a new technology for the production of microcapsules based in atomization processes. *Chem Eng J*. 2006;117:137–142.
29. Del Gaudio P, Colombo P, Colombo G, Russo P, Sonvico F. Mechanisms of formation and disintegration of alginate beads obtained by prilling. *Int J Pharm*. 2005;302:1–9.
30. Seifert DB, Phillips JA. Production of small, monodispersed alginate beads for cell immobilization. *Biotechnol Prog*. 1997; 13:562–568.
31. Lefebvre AH, editor. *Atomization and Sprays*. New York: Hemisphere Publishing Corporation, 1989.
32. Weber C. Zum Zerfall eines Flüssigkeitsstrahls. Zeit für angewandte Mathematik und Mechanik. 1931;11:136–141.
33. Hanif H. *Formation and Break Up of Microscale Liquid Jets*. Georgia Institute of Technology, 2009.
34. Chigier N, editor. *Spray Technology Short Course*. Pittsburgh, Pensylvania: Carnegie Mellon University, 1995.
35. Adelberg M. Breakup rate and penetration of a liquid jet in a gas stream. *AIAA J*. 1967;5:1408–1415.
36. Mansour A, Chigier N. Air-blast atomization of non-Newtonian liquids. *J Non-Newtonian Fluid Mech*. 1995;58:161–194.
37. Adelberg M. Mean drop size resulting from the injection of a liquid jet into a high-speed gas stream. *AIAA J*. 1968;6:1143–1147.
38. Jeffreys H. On the formation of water waves by wind. *Proc R Soc London, Ser A*. 1925;107:189–206.
39. Mayer E. Theory of Liquid Atomization in Hugh Velocity Gas Streams. *ARS J*. 1961;31(12):1783–1785.

Manuscript received Oct. 15, 2010, and revision received Jan. 3, 2011.